Materials and Design 100 (2016) 141–150

Contents lists available at ScienceDirect

Materials and Design

journal homepage: www.elsevier.com/locate/matdes

Cyclic pressure on compression-moulded bioresorbable phosphate glass fibre reinforced composites

Fernando Barrera Betanzos *, Miquel Gimeno-Fabra, Joel Segal, David Grant, Ifty Ahmed

University of Nottingham, Department of Materials, Mechanics and Structures, Nottingham, UK

ARTICLE INFO

Article history:
Received 18 January 2016
Received in revised form 17 March 2016
Accepted 19 March 2016
Available online 21 March 2016

Keywords:
Bioresorbable composites
Phosphate glass fibre
Polylactic acid
Cyclic pressure

ABSTRACT

The use of thermoplastic composites based on poly(lactic) acid and phosphate glass fibres over metallic alloys for clinical restorative treatment is highly beneficial due to their biocompatibility and biodegradability. However, difficulties in achieving a thorough melt impregnation at high fibre contents while limiting polymer degradation is one of the main issues encountered during their manufacture. This paper reports for the first time on the effects of pressure cycling on the mechanical properties of compression moulded polylactic acid-phosphate glass fibre composites. The strength of the composites consolidated under pressure cycling were at least 30% higher than those in which conventional static pressure was used. The marked disparity was attributed to the influence of pressure cycling on the fibre preform permeability, the melt viscosity and the capillary pressure, leading to improved fibre wet-out with respect to static pressure. Implementation of a cyclic pressure appeared to promote the occurrence of transcrystallinity in the polymer matrix as suggested by DSC traces. The fibre content influenced PLA thermal degradation since the matrix molecular weight decreased as the fibre content increased on account of the moisture adsorbed by the glass surface. However, this extent of degradation did not impair the matrix mechanical performance in the composites.

1. Introduction

Bone atrophy due to stress shielding associated with metallic fixation devices can result in secondary surgery for removal of these implants to prevent long term complications. As such, current research efforts have been focused on the development of novel fully bioresorbable devices capable of eliciting beneficial host responses post-implantation [1–3].

Long-fibre composites fabricated from biodegradable materials, such as polylactic acid 'PLA' and phosphate-based glass fibres 'PGF' can be engineered to initially match (and even surpass) bone mechanical properties and gradually transfer the load to the healing tissue upon degradation. Furthermore, the controlled release of phosphate glasses degradation by-products could stimulate the fracture healing mechanism following in situ degradation [4,5].

Amongst the factors that regulate the loading response of composite materials, the fibre content and the adhesion between the matrix and the reinforcement play a critical role [6,7]. From Darcy's law [7], it follows that the higher the viscosity of the polymer melt and the thicker the porous medium, i.e. the higher the fibre volume fraction, the more difficult would be for a given fluid to fully percolate through the interstices of the fibre network.

Intimate interfacial contact is vital not only to fully exploit the strength and stiffness of the reinforcement through effective stress transfer, but also to minimise void content. Voids are detrimental to the composite mechanical properties, due to their action as stress risers and the reduction of the effective matrix-fibre contact area [8]. Moreover, their presence expedites water diffusion, accelerating the loss of mechanical properties in in aqueous environments [9].

As a consequence of the high melt viscosity of PLA (and with thermoplastics in general, 100–1000 Pa s [10]), poor quality composites often result from laminates with high fibre to matrix ratio, ultimately hindering the orthopaedic usage of fibre reinforced bioresorbable composites. Conventional approaches utilised in the composite industry to tackle this issue have been: i) the adoption of higher temperatures to reduce the matrix viscosity (enhancing flowability) and ii) increases in the product residence time [11]. Since polylactic acid is a thermally labile thermoplastic which can undergo a rapid loss of molecular weight at temperatures higher than the melting point [12,13], increases in the processing temperature and/or protracted moulding cycles are detrimental to the composite performance.

Alternatively, the consolidation pressure during part forming could be increased to aid in the polymer melt infiltration through the fibre network. However, the fundamental drawback with the increase of pressure is the further compaction of the fibre array, which compromises both the fibre bed permeability and the evacuation of entrapped

* Corresponding author.

http://dx.doi.org/10.1016/j.matdes.2016.03.108

air [7,14]. Therefore, statically applied pressure only has had a limited success in the efficient production of void-free high quality parts with consistent performance under loads (especially at high fibre contents).

In this study it was hypothesised that the implementation of an active pressure profile during part consolidation could address the difficulties imposed by the high polymer viscosity in an extensively used manufacturing technology as compression moulding. This paper reports on the effects of a dynamic compression moulding variant for the production of high volume fraction laminate bioresorbable composites aiming to: i) limit the PLA matrix thermal degradation, ii) minimise void content and iii) significantly improve composite mechanical properties through the optimisation of the pressure scheme applied.

2. Materials and methods

2.1. Melt-drawn fibre spinning and fibre preform production

Phosphate glass fibres of the composition $45P_2O_5$-16CaO-$13Na_2O$-$24MgO$-$2Fe_2O_3$ mol.% and a diameter of 20 ± 2 μm were continuously drawn at 30 ms^{-1} directly from a glass melt using an in-house melt-drawing facility. The parent glass was synthesised from reagent grade NaH_2PO_4, $CaHPO_4$, $FePO_4 \cdot 2H_2O$, P_2O_5 and $MgHPO_4 \cdot 3H_2O$ (Sigma Aldrich, UK) powder precursors which were mixed into a Pt/5% Au crucible (Birmingham Metal Co., UK), and then placed in a furnace for 30 min at 350 °C to allow the powders to dry. The crucible was then transferred to a furnace preheated at 1150 °C for melting. A 90 min period was allowed for melt homogenisation. Finally the melt was poured onto a steel plate and left to cool to room temperature.

Non-woven unidirectional 'UD' plies were manufactured by drawing fibre onto a traversing drum. The fibres were then sprayed to prevent fibre misalignment using a 5 g/100 mL PLA-Chloroform solution (Resin Ingeo 3251-D NatureWorks®). Following a 2 h period for the complete evapouration of the chloroform, the ply was cut into 121 cm^2 square pieces for subsequent processing. The mass of the plies used for the fabrication of composites with different fibre volume fractions are listed in Table 1.

To be able to assess the degree of impregnation achieved by the respective manufacturing technique, the composites were fabricated from progressively thicker plies as detailed in Table 1.

2.2. Single fibre tensile test

The tensile properties of 60 fibres with a gauge length of 25 mm were evaluated through uniaxial tensile test of individual filaments using a LEX810 Tensile Tester according to standard BS ISO11566. The fibres were randomly selected from a freshly drawn bundle. Prior to testing, the fibre diameter was determined with a Mitutoyo Series 544 LSM-500S Laser diameter gauge.

Evaluation of the tensile strength was conducted using Weibull's statistics assuming a uniform distribution of independent flaws. Weibull parameters were calculated using Minitab® 15 (version 3.2.1).

2.3. Fibre density measurements

Glass fibre density measurements were obtained via use of a AccuPycTM 1330 Pycnometer with a precision of 0.1% calibrated using a standard steel sphere. Fibre density variability was ± 0.02 g cm^{-3}. The analysis was repeated 10 times and the mean value was used for the relevant calculations.

Table 1
Composition of the laminates assembly to achieve the target volume fractions.

Sample codes	v_f	PLA mass (g)	PGF mass (g)	Plie mass (g)	No. of plies
PLA-plate	0	67.31	–	–	–
Vf-15	0.15	57.21	21.35	1.33	16
Vf-25	0.25	50.48	35.58	2.54	14
Vf-35	0.35	43.75	49.81	4.15	12
Vf-45	0.45	37.02	64.04	6.40	10

2.4. Composite manufacturing

PLA films of ca. 0.3 mm in thickness were fabricated by pressing 4.5 g batches of PLA resin pellets (Resin Ingeo 3251-D NatureWorks®). The PLA pellets were dried in a vacuum oven at 50 °C for at least 24 h prior use and were then placed between two PTFE covered aluminium plates. The plates were then transferred a hydraulic press preheated to 185 °C. The pellets were held at this temperature for 5 min before compressing at 3 bar for 10 s. Finally the plates were then moved to a second press set at the same pressure for cooling. The PLA films were then trimmed, bagged and stored in a vacuum oven for post-composites at different stages during the manufacturing processes and fibre content processing.

Two series of unidirectional composites of four nominal volume fractions v_f (see Table 1) were manufactured by alternately stacking layers of PGF plies and PLA films inside a purpose-built compression moulding tool with a 4.5 mm × 110 mm × 110 mm (thickness × width × length) cavity. The mould was placed in a hydraulic press at 180 °C for 10 min as shown in Fig. 1. Immediately after, the pressure was alternated between 40 and 0 bar for 1 min to assist the evacuation of air trapped during the lay-up, followed by consolidation for 9 min according to two different pressure schemes illustrated in Fig. 1: a) static pressure 'SP' (pressure held constant at 40 bar throughout the 9 min) and, b) cyclic pressure 'CP' (pressure cycled for 1.5 min towards the end of the consolidation stage). Finally the system was cooled under constant pressure to prevent cavitation from crystallisation or thermal shrinkage of the polymer melt.

For each nominal fibre volume fraction in the respective series, at least two composites were fabricated. In addition, pure PLA plates were fabricated from film laminates as control samples.

2.5. 3-Point bending test

Samples of 4.5 mm × 15 mm × 90 mm (thickness × width × length) PLA and composite plates were characterised through 3-point bending test in accordance with BS EN ISO 14125:1998 standard. Three samples for each composite fabricated were tested using a Hounsfield Series S testing machine with a cross-head speed of 1 mm min^{-1}, and a 5 kN load cell.

2.6. Scanning Electron Microscopy (SEM)

The 3-point bending test coupons were mounted in epoxy resin, polished and sputter coated with platinum and examined using a Philips XL-30 scanning electron microscope with an accelerating voltage of 10 kV in secondary electron mode.

2.7. Differential Scanning Calorimetry (DSC)

The thermal properties of the composite's polymer matrix were determined with a DSC Q10 (TA Instrument, USA). Prior to use the equipment was calibrated with mercury and indium standards. Thin composite slices, cut in the transverse direction using a diamond saw, were loaded into sealed aluminium pans and heated under nitrogen flow of 50 cm^3 min^{-1} from 30 °C to 190 °C at a rate of 5 °C min^{-1}. A 5 min isothermal hold was allowed before cooling at a rate of 20 °C min^{-1} back to 30 °C. The equipment was allowed to equilibrate at this temperature before resuming a subsequent run with the same parameters as those previously described.

On account of the fibre content, the mass of the composite slices was adjusted according to their experimental volume fraction to keep the polymer matrix mass constant at ca. 13 mg. The samples were dried under reduced pressure for 48 h (0.01 mbar) at 30 °C and stored in a

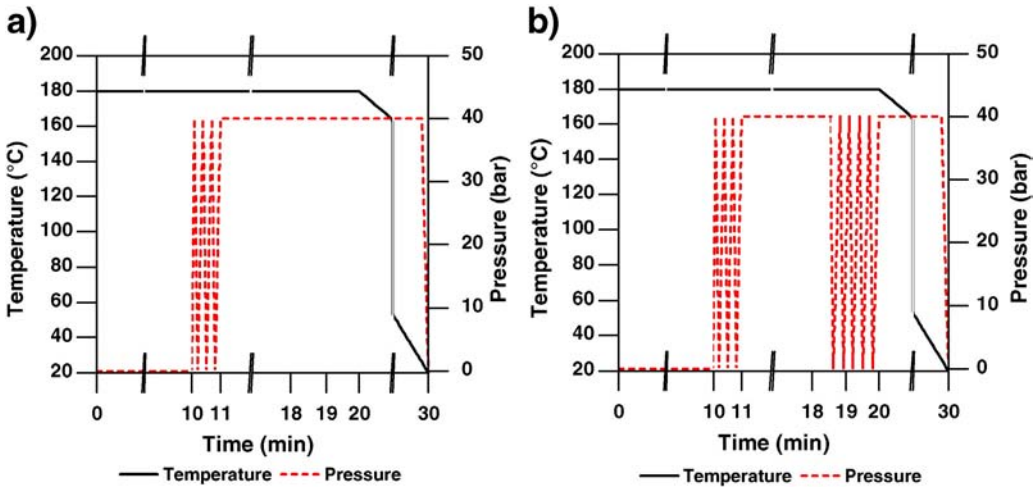

Fig. 1. Schematic representation of the nominal thermal and pressure processing schemes for the PLA-PGF composites: a) static pressure case and b) cyclic pressure case.

desiccator until use. The DSC traces were analysed using TA instrument universal analysis 2000 software version 4.3A. The crystallinity content '*X*' of the samples was evaluated using Equation (1) [15]:

$$X\% = \frac{100(\Delta H_m - \Delta H_c)}{\Delta H_m^0} \quad (1)$$

where ΔH_m and ΔH_c are the melting and crystallisation enthalpies, respectively, and ΔH_m^0 is the reference melting enthalpy for PLLA crystals having an infinite size ($93.6\ J\ g^{-1}$) [15].

2.8. Void content determination

Due to the hygroscopic nature of both fibres and PLA, the composite samples were conditioned in a vacuum oven at 40 °C to remove any absorbed moisture until constant weight was achieved. The percentage void content φ_v, of the composite coupons (no smaller than 2 cm^3) was measured by the standard loss on ignition method (detailed in ASTM D-2734-09) using a minimum of three samples in accordance with Equation (2) [16]:

$$\varphi_v = \frac{100(\rho_{ct} - \rho_{ce})}{\rho_{ct}} \quad (2)$$

where ρ_{ce} stands for the sample experimental density and ρ_{ct} is the composite theoretical density given by Equation (3) [16],

$$\rho_{ct} = \frac{1}{{}^{w_m}/_{p_m} + {}^{w_f}/_{p_f}} \quad (3)$$

w_m and w_f being the matrix and glass fibre mass fraction and p_m and p_f being the fibre and matrix density.

The experimental density of the composite samples, ρ_{ce}, was determined in accordance with the standard ASTM D-792, from the weight difference of samples in air and ethanol at 23 °C, as shown by Equation (4) [17]:

$$\rho_{ce} = \frac{A}{A-B}(\rho_e - \rho_a) + \rho_a \quad (4)$$

where *A* and *B* are the weight of the sample in air and submerged in ethanol and ρ_e and ρ_a are the density of ethanol and air at the operating temperature (0.789 g cm^{-3} and 0.0012 g cm^{-3} at 23 °C respectively). The weight of the immersed sample was averaged over four measurements and used in Equation (4).

After volatilisation of the organic component, the real volume fraction was calculated using Equation (5) according to ASTM D2584-11 [18]:

$$v_f = \frac{{}^{w_f}/_{p_f}}{{}^{w_m}/_{p_m} + {}^{w_f}/_{p_f}}. \quad (5)$$

2.9. Advanced polymer chromatography (APC)

The PLA matrix thermal degradation was evaluated using a Waters ACQUITY advanced polymer chromatography (APC™) system, coupled with a refractive index 'RI' detector. Separation was achieved by a column bank consisting of Waters Aquity XT 125 (Effective molecular weight range 1000–30,000 g/mol) and XT 450 columns (Effective molecular weight range 20,000–400,000 g/mol), each having 4.6 mm internal diameter and 150 mm length. The isocratic mobile phase was chloroform, injection volume was 30 μL, the flow rate was 0.3 mL/min and the temperature of the column bank and detector was 30 °C. The calibration curve was obtained by using 3 different polystyrene standards (Waters ReadyCal Kit).

3. Results

3.1. Flexural properties

The experimental mechanical and physical properties of the composite constituent phases, used in the relevant calculations, were compiled in Table 2. Figs. 2 and 3 depict the flexural properties of the composite plates manufactured via the different pressure profiles as detailed in the Materials and Methods section. The error was computed as standard deviation.

The flexural properties in both composite series greatly exceeded those of PLA alone (75 ± 3 MPa for flexural strength and 3.3 ± 0.4 GPa for modulus respectively). Flexural strengths for the CP-

Table 2
Physical and mechanical properties of composite constituent phases.

Properties	Phosphate glass fibre	Polylactic acid
Density (g cm^{-3})	2.640 ± 0.005	1.250 ± 0.002
T_g (°C)	462 ± 1	55–60[a]
T_m (°C)	840 ± 1	155–170[a]
Strength (MPa)	700 ± 250	75 ± 3
Modulus (GPa)	61 ± 5	3.3 ± 0.4
Elongation at break (%)	1.5 ± 0.7	3.5 ± 0.3

[a] Physical parameters acquired from the manufacturer technical data sheet.

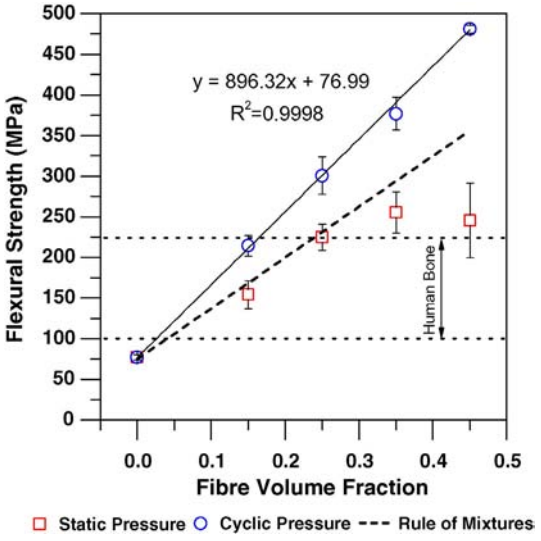

Fig. 2. Influence of the pressure profile on composites flexural strength with progressively higher fibre content (error bars indicate ± standard deviation). The black dashed line represents the theoretical composite strengths calculated using mean experimental matrix and fibre strengths in the rule of mixtures. The range of human bone flexural strength is denoted by black dotted lines.

composites closely followed a linear profile as demonstrated by the correlation coefficient, R^2 (ca. 0.99) shown in Fig. 2.

For all volume fractions, the strength values of the CP-composites significantly surpassed those of the SP-series; the difference being more pronounced the higher the fibre contents. This was clearly evident for the 0.45 v_f samples, where a 250 MPa difference was observed separating the mean strength values of both composite series.

For comparison purposes, the strength values of a PLA-PGF composite series were calculated from the mean experimental strengths of the constituent phases (cf. Table 2) using the rule of mixtures, expressed by Equation (6) [19]:

$$\sigma_c = \sigma_f v_f + \sigma_m(1 - v_f) \tag{6}$$

where σ_c, σ_f and σ_m are the composite, fibre and matrix strengths

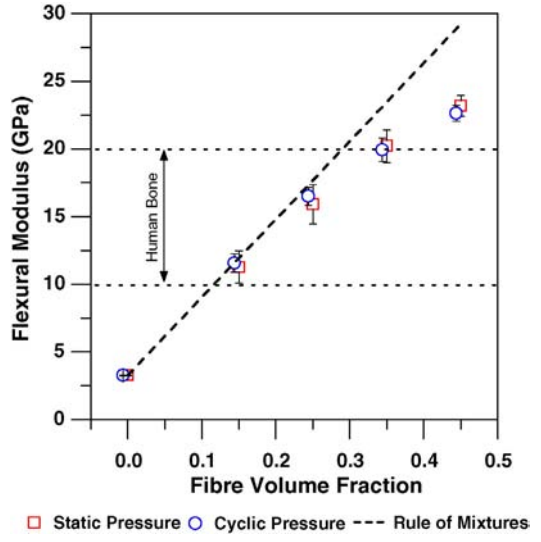

Fig. 3. Influence of the pressure profile on composites flexural modulus with progressively higher fibre content. The black dashed line represents the theoretical composite moduli calculated using mean experimental matrix and fibre moduli in the rule of mixtures. The range of human bone flexural modulus is denoted by black dotted lines.

respectively. The results were graphically illustrated by the black dashed line in Fig. 2.

The strength profiles for the 0.15 v_f and 0.25 v_f static pressure samples are well approximated by the predicted rule of mixtures curve. However, from the 0.25 v_f composite onwards, further increases in fibre content did not result in a strength improvement as estimated, but instead deleteriously impacted the consistency of the strength values as shown by the large standard deviation values attained.

On the other hand, the strengths of the cycled pressure composites exceeded the values predicted by the rule of mixtures curve in all cases and described a well-defined linear trend with a greater slope.

An estimate of the effective strength of both matrix and fibres in the CP-composite series can be gained by rewriting Equation (6) into the slope-y intercept form of a linear equation with v_f as the independent variable and σ_m as the y-intercept:

$$\sigma_c = v_f(\sigma_f - \sigma_m) + \sigma_m. \tag{6.1}$$

By equating the slope and y-intercept values of the best fitting line describing the trend of the CP-composites strengths (solid black line in Fig. 2) to the correspondent terms in (6.1), values of ca. 77 MPa and ca. 973 MPa were obtained for the matrix and fibre effective strength respectively in the cycled pressure-composite system.

The matrix strength value at the ordinate intercept was found to be similar to the experimental strength of PLA (75 ± 3 MPa) shown in Table 2. However, the effective fibre strength was found ca. 40% higher than the experimental fibre strength value associated with the SP series.

No substantial differences in the modulus values were observed between the CP and SP-composites series. The elastic modulus increased with fibre additions. It was observed that the 0.15 v_f and 0.25 v_f samples complied with the rule of mixtures applied to modulus, however the higher fibre volume fractions, namely the 0.35 and 0.45, diverged to lower values.

3.2. Differential Scanning Calorimetry

Representative DSC traces from the second heating cycle for the composites fabricated are depicted in Fig. 4. Four features can be readily distinguished in the DSC thermograms: i) a glass transition phenomenon T_g, ii) a cold crystallisation peak (of which the maximum temperature T_{X1} and onset of crystallisation X_0 are reported in Table 3), iii) a polymorphic transition peak (denoted by T_{X2}) and iv) an endothermic peak (characterised by T_m) associated with the melting of crystalline phases. The enthalpies of melting ΔH_m and crystallisation of both peaks ΔH_{X1} and ΔH_{X2} respectively, are also listed in Table 3 along with the crystallinity content calculated as referred in the Materials and methods section. No distinctive features could be observed in the DSC traces upon cooling.

Differences in the thermal behaviour between the composites of the two series and the control PLA plate were readily identified, as summarised in Table 3.

In the cycled pressure composite series, the most noticeable changes observed following the incorporation of fibres into the polymer matrix were: i) the contraction of both the melting and the cold crystallisation peak roughly at the same rate, resulting in a constant and rather low crystalline content throughout the composite series, (see Table 3), ii) the broadening of the crystallisation peak as a result of the evolution of a shoulder which appeared to intensify as the fibre content increased, and iii) the progressive shift of the crystallisation peak towards lower temperatures as the fibre content increased.

The melting and the cold crystallisation peaks for the SP composites also changed upon fibre addition in similar fashion to that previously described for the CP-series, but to a lesser extent. Both the onset and the maximum peak temperature shifted to lower temperature with the addition of fibres. No significant changes in the glass transition temperature were found.

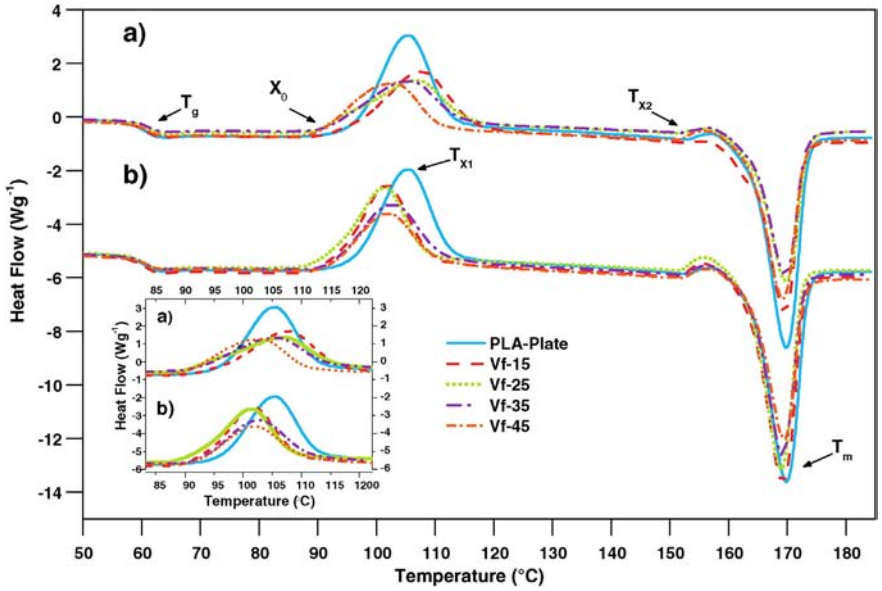

Fig. 4. DSC traces of representative samples of a) cycled pressure and b) static pressure composite series. Insert shows an enlarged view of the cold crystallisation peaks for both composite series.

To rule out the possible effect of molecular weight decrease on the PLA crystallisation, the thermal cycle described in section 2.7 was repeated in selected samples up to four times. No significant differences could be found between these complementary runs.

3.3. Void content analysis

The results of the composite void content analysis conducted through comparison of the experimental and theoretical density values were outlined in Table 4. With the exception of the 0.45 v_f SP specimens (where a threefold increase in void quantity was attained in comparison with the correspondent CP composite samples) low void-content ($\varphi_v < 1\%$) composite specimens were achieved for both pressure profiles. The void content proved not to be dependent on the manufacturing method up to 0.35 v_f, with only a minor tendency for pressure cycling to produce composites with less voids.

Fig. 5 shows the cross section of the 0.35 v_f and 0.45 v_f composite specimens fabricated via static (left) and cyclic (right) pressure profiles. A crack, resultant of flexural testing that propagated through the interface between the polymer and the fibre can be distinguished in Fig. 5b. No significant differences were observed between the cross sectional images of the 0.15 v_f and 0.25 v_f samples fabricated under different pressure conditions and therefore not shown in here.

It was noticed that voids were concentrated at the interstices between the fibres mainly at the centre of the UD fibre mats. No such defects could be seen in the polymer rich zones amongst the plies. In the case of the 0.35 v_f specimens (obviating the crack) a marginally higher number of voids can be observed in the SP specimen (Fig. 5a).

The difference in the effect of the pressure variation was more evident as the effective thickness of the fibre preform increased. Only a few voids were observed in the 0.45 v_f CP cross section image in Fig. 5d, whereas large voided areas were present at the centre of the fibre plies in the 0.45 v_f SP sample fabricated under static pressure (Fig. 5c).

3.4. Advanced polymer chromatography

Molecular Weight Distribution results are shown in Table 5. The number average M_n, weight average M_w, the *Z*-average molecular weight M_z, and the calculated polydispersity index $Đ_M$, are shown for the polymeric matrix in the PLA-PGF composites at different stages during the manufacturing processes and fibre content. The molecular weight results for both pressure profiles were found identical within

Table 3
Thermal properties of PLA-PGF composite plates.

Cycle	Specimen	Pressure profile	T_g (°C)	X_0 (%)	T_{X1} (°C)	T_{X2} (°C)	T_m (°C)	ΔH_m (J g^{-1})	ΔH_{X1} (J g^{-1})	ΔH_{X2} (J g^{-1})	$\%X_c$ (%)
2	PLA-plate	NA	58.5	96.4	105.2	157.0	169.8	44.01	43.56	0.75	0.48
	0.15	CP	58.6	95.0	108.1	156.3	169.6	37.03	36.89	0.36	0.15
	0.25		59.5	91.0	107.1	156.3	169.8	33.47	33.30	0.57	0.18
	0.35		59.6	91.6	106.2	156.9	169.7	30.22	30.08	0.83	0.15
	0.45		59.7	90.5	105.6	156.7	170.0	28.64	27.47	0.96	1.25
	0.15	SP	58.5	93.1	101.9	156.3	169.3	41.15	39.39	2.31	1.88
	0.25		58.4	92.0	101.2	156.3	170.0	38.71	36.93	2.15	1.90
	0.35		59.2	92.3	102.8	156.9	170.2	35.05	32.89	1.99	2.31
	0.45		59.1	92.2	102.3	156.9	169.5	30.72	28.38	1.78	2.50
1	PLA-plate	NA	62.4	95.6	106.2	157.5	171.5	45.49	43.24	0.68	2.40
	0.15	CP	62.8	93.6	109.9	156.0	170.9	37.94	35.88	0.30	2.20
	0.25		60.7	88.9	109.1	155.8	171.0	33.88	29.75	1.32	4.41
	0.35		60.0	88.2	104.4	155.4	170.0	31.04	25.91	0.62	5.48
	0.45		58.7	87.4	104.2	155.8	170.1	29.49	25.09	1.05	4.70
	0.15	SP	61.2	92.8	103.6	156.7	170.4	41.62	37.03	1.23	4.90
	0.25		64.0	90.4	102.6	156.4	170.4	38.88	32.51	1.32	6.81
	0.35		61.9	90.7	103.8	156.6	170.6	34.76	29.46	1.03	5.66
	0.45		61.6	90.4	102.27	156.23	169.64	30.81	23.85	1.116	7.44

Table 4
Summary of composite volume fraction and void content analysis.

v_f nominal	Pressure profile	ρ_{ce} (g cm^{-3})	v_f experimental	φ_v (%)
0.15	SP	1.460 ± 0.010	0.150 ± 0.006	0.370 ± 0.020
	CP	1.460 ± 0.020	0.160 ± 0.010	0.320 ± 0.030
0.25	SP	1.590 ± 0.030	0.240 ± 0.020	0.250 ± 0.020
	CP	1.610 ± 0.005	0.260 ± 0.004	0.140 ± 0.050
0.35	SP	1.700 ± 0.040	0.340 ± 0.030	0.540 ± 0.150
	CP	1.740 ± 0.007	0.360 ± 0.003	0.540 ± 0.130
0.45	SP	1.840 ± 0.020	0.450 ± 0.010	1.900 ± 0.600
	CP	1.870 ± 0.010	0.460 ± 0.010	0.730 ± 0.040

Table 5
Summary of Molecular Weight results for the materials used.

Specimen	M_n (g mol^{-1})	M_w (g mol^{-1})	M_z (g mol^{-1})	$Đ_M$
Virgin	121,000 ± 700	158,000 ± 1000	216,000 ± 1500	1.311
Film	116,000 ± 800	154,000 ± 1100	212,000 ± 1600	1.325
Plate	115,000 ± 1900	155,000 ± 460	213,300 ± 350	1.340
Vf-15	115,300 ± 700	150,000 ± 1000	203,000 ± 1700	1.302
Vf-25	113,100 ± 1000	146,500 ± 750	195,000 ± 3000	1.300
Vf-35	104,000 ± 2000	135,000 ± 2000	179,000 ± 800	1.300
Vf-45	97,000 ± 600	121,000 ± 500	153,000 ± 800	1.250

experimental error and thus generic molar masses for the composites are reported in the following.

From the data presented in Table 5 it can be appreciated that the molecular weight tends to decrease steadily throughout the sequential processing steps of laminate compression moulding. Furthermore the fibre content seems to have a deleterious effect on the molar mass during melt processing since the higher the volume fraction, the lower the molecular weight.

The polydispersity index roughly maintained constant during sequential processing steps and for different fibre volume fractions.

4. Discussion

Melt processing is a widely used technique at the industrial level for the manufacture of thermoplastic products and its fibre reinforced variants [20]. One of the main issues that precludes fibre reinforced thermoplastic products from structural applications, is the difficulty in achieving thorough melt impregnation using conventional equipment without inducing considerable fibre attrition or significantly degrading the matrix consequent to long term exposures to high temperatures. Therefore, alternate approaches to alleviate the viscosity hindrance other than those relying on high temperature and/or high stresses, such as the pressure cycling method presented here, are likely to enhance the composite performance and pave the way for product adoption.

The absence of air bubbles in the regions adjacent to the top and bottom surfaces of the fibre mats (Fig. 5) and the overall low void contents calculated for both pressure profiles indicated that the initial application of cyclic pressure managed to successfully eliminate large pockets of entrapped air and vapour possibly stemming from moisture adsorbed during mould loading.

Typically for each 1% increase in void content, the mechanical properties (tensile, flexural and compressive) show ca. 7% a reduction [21–24]. Considering the analogous, and rather low void contents (listed in Table 4) calculated for the composite specimens, the substantial difference observed in flexural strengths (going from ca. 30% for the 0.15, 0.25 and 0.35 volume fractions up to ca. 50% in the 0.45 v_f sample) cannot be solely based on the detrimental effects of macroscopic voids.

The effective fibre strength in the CP-system (ca. 950 MPa) was 36% higher than that associated with the SP composites series (700 MPa). Such a difference is suggested to arise at least partly from the superior degree of impregnation achieved by cycling the applied pressure, and the associated reduction in the interstitial areas of trapped air between individual filaments (microvoids) [24,25]. This is better illustrated in the case of the 0.45 v_f composites. Poor fibre-matrix contact resulted in the large voided areas observed in the cross section of the 0.45 v_f SP composite (Fig. 5d). Conversely, no such defects can be observed in the cross section of the 0.45 v_f composite consolidated under cyclic pressure (Fig. 5c).

As schematically shown in Fig. 6, the application of hydrostatic pressure acts to increase the packing of fibres and thus, hinders the percolation of the polymer through the micron-sized gaps between filaments [24,26,27]. Due to viscoelastic response of the polymer melt, the stresses induced by the application of pressure gradually relax, as does the fibre agglomeration allowing a partial recovery of the fibre network

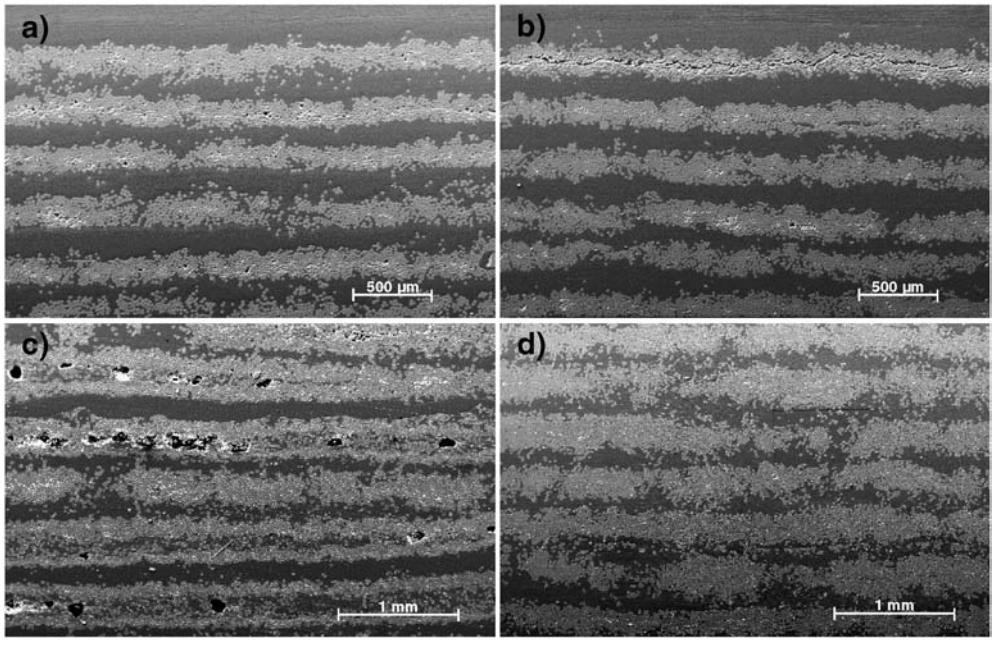

Fig. 5. (Top) SEM cross sectional images of the 0.35 volume fraction composites manufactured by a) static pressure and b) cyclic pressure profiles. (Down) SEM cross sectional images of the 0.45 volume fraction composites manufactured by c) static pressure and d) cyclic pressure profiles.

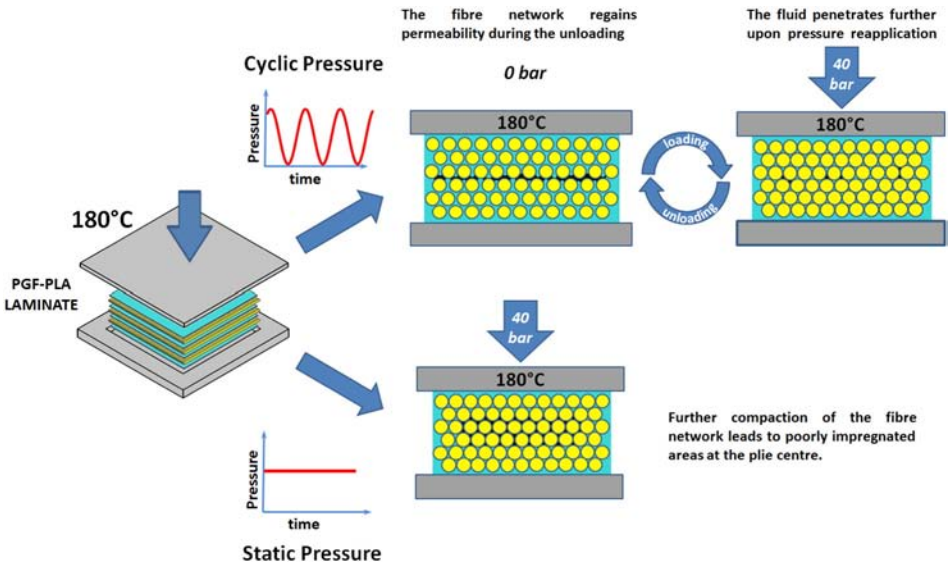

Fig. 6. Schematic description of the consolidation process under cyclic and static pressure.

permeability and penetration of the polymer melt. Viscous relaxation inevitably causes a gradual reduction in pressure-driven melt penetration, limiting the fibre wet-out efficiency of the static pressure profile.

However with the implementation of cyclic pressure, the recovery of the fibre mat permeability may occur during the unloading part of the pressure cycle (refer to Fig. 6). Therefore, when the loading is reapplied, the pressurised fluid percolates more readily through the interstices in the fibre network. This process was repeated in successive cycles, leading to discrete polymer percolation steps which rendered an overall superior fibre wet-out in the cycled pressure composite series when compared to its static counterpart.

Another advantage of cyclic pressure is its ability to compensate for adverse capillary effects. As the flow front advances, the air volume is progressively reduced, leading to the development of an internal back pressure in the remaining voids that counters the externally applied one [24]. At this stage, further penetration of the polymer melt would then be controlled mainly by capillary forces as a result of the reduction in the applied pressure.

In systems where the contact angle is greater than zero due to the incompatibility of the phases (as is the case of the hydrophilic bioactive glass surfaces and the hydrophobic poly(α-hydroxyacid) melts [28,29]), the capillary pressure tends to oppose further resin penetration [30]. Consequently, in composite systems where only static pressure has been implemented, a considerable amount of entrapped air will remain at the centre of the fibre bed in the form of elongated bubbles, which preferentially concentrate adjacent to the fibres under surface tension considerations. It was expected that the longer the diffusion path of the penetrating fluid, the more severe the concentration of residual air will be.

In contrast to the static case where relaxation of the applied pressure is slow, with cyclic pressure the entrapped gas volume is able to quickly change in response to the alternating motion and reduce the opposing capillary pressure. Since the restraints imposed by the surrounding medium relax in the course of the unloading part of the cycle, the elongated air bubbles can reduce their surface energy by coalescing and adopting a spherical shape. As the pressure is reapplied during the loading part of the cycle, the highly stable spherical bubbles resists being deformed and are forced to abandon the interstices between neighbouring fibres.

Additionally, due to the pseudoplastic behaviour of PLA in response to an increase in the shear force [31,32], the application of cyclic pressure may induce a redistribution of shear stresses in the melt, leading to a local alignment of the polymer chains with the concomitant reduction of the apparent melt viscosity, ultimately allowing easier percolation through the fibre network interstices. Recent publications on augmented injection moulding process have suggested that an altered rheological state can be induced in non-Newtonian fluids through the application of oscillatory forces [33–36]. However, since the early study of Barnes et al. [37] it was known that the induction of pulsed sinusoidal pressure gradients with non-zero means resulted in superior flowability of a non-Newtonian fluid causing a reduction in melt viscosity due to the inducement of shear-thinning.

The augmented impregnation quality and the concomitant enhanced densification through combination of the above combination of mechanisms accounted for the higher flexural strengths of the CP-composites series. Furthermore, the physical effects of cycled pressure in this study resulted in the highest hitherto reported mechanical properties for PGF-PLA composites [38–41]. The mechanical properties of the cycled pressure-composites were even found to be 26% and 45% greater to those cases where the fibre surface had been respectively treated with 3-aminopropyltriethoxysilane and sorbitol ended PLA oligomers to improve the fibre-matrix adhesion in a recent study [42].

The similarity in modulus for both composite series indicated that, contrary to the flexural strength, the flexural modulus was less sensitive to the presence of interfacial defects in agreement with previous studies [22,43]. This was expected since the composite elastic response result from volume-averaged stress and strain fields [44]. On the other hand, matrix dominated properties like the flexural strength are influenced by the location of defects throughout the cross section as a result of the non-uniform stress distribution in bending [43]. Nonetheless, the divergence from the theoretical behaviour described by the rule of mixtures (Fig. 3) in the 0.35 and 0.45 v_f cases, suggested that the dominating factor for the observance of maximum stiffness values could be ascribed to the distribution of the reinforcement throughout the entire cross section.

To better evaluate the impregnation efficiency of both methods, the laminates were assembled from progressively thicker fibre mats. As a result, the reinforcements were increasingly segregated in fibre rich zones as the nominal volume fraction increased. Therefore, the presence of polymer rich zones and fibre clustering gave rise to modulus values lower than those theoretically achievable since prediction of modulus is dependent a uniform distribution of the reinforcement throughout the entire matrix [45]. Similar effects of the laminating composition on the composite modulus have been reported for compression moulded PLA-PGF composites [40].

It has been shown that the improvement gained by the incorporation of reinforcements can be one order of magnitude greater for

semi-crystalline matrices than for amorphous ones [46]. Such a difference was attributed to the occurrence of a transcrystalline layer around the reinforcement as a result of high heterogeneous nucleation ability of the fibre surface [47–49]. A transcrystalline interphase is thought to perform as a strong mechanical interlock, improving the stress transfer between fibre and matrix particularly in composites with poor matrix-fibre interfacial adhesion as the PLA-PGF system [48]. Previous investigations in polymer processing have demonstrated that one of the effects of the in-mould manipulation is the change in the crystallisation kinetics and the resultant crystal morphology of the product [50,51]. The DSC studies here were conducted to evaluate the changes operated in the composites consequent to the application of cyclic pressure.

As illustrated by Table 3 (cf. $\%X_c$ in cycle 1), crystallinity developed upon cooling during manufacture of both composite series [52], the extent of which was greater for the SP samples. Decreases in the molecular weight have been shown to significantly affect the crystallisation of PLA as a result of the increased mobility of shorter polymer chains, however these increases in diffusion were found negligible in samples with molecular weights in the range of 10^5 g mol^{-1} or higher [53,54]. Therefore, the crystal content increase in proportion to the fibre volume fraction for both composite series can be attributed to the nucleation and growth of crystals favoured by the fibre surface. In spite of the low crystallinity content (maximum ca. 5.5%), its occurrence could be significant to the mechanical properties of the fibre reinforced composite if located at the fibre-matrix interface.

The shift of the crystallisation peak and the progressive evolution of a shoulder in the low temperature side for the CP composite series evidenced the heterogeneous nucleation ability of fibres, which reduced the thermal energy barrier for nucleation and crystal growth upon heating. Such a shoulder, absent in the neat PLA sample, has been attributed to a crystallisation kinetics decay once the growth of surface nucleated spherulites is limited to directions perpendicular to the fibre surface by steric hindrance, giving rise to a transcrystalline layer [55,56]. The transcrystalline envelope continues to grow until further development was hindered by impingement with bulk spherulites, after which the crystallisation rate rapidly declined.

No such shoulder was observed on the crystallisation peaks of the composites in the whole SP series. All the peaks equally shifted towards lower temperatures and exhibited a shape analogous to that of neat PLA. The close resemblance of the crystallisation peaks in the SP composites to that of neat PLA (experiencing shrinkage due to less availability of polymer matrix in proportion to the fibre content) and the peak displacement were indicative of the absence of transcrystallinity in these samples, in favour of bulk spherulites. This result agreed with previous findings where unsized glass fibre was denoted as a rather poor transcrystallinity former under quiescent conditions in various composite systems [57,58].

The difference in matrix crystallisation behaviour upon heating and its persistence after remelting in this study suggested a local chain alignment consequent to the application of cyclic pressure. This configuration might be stabilised in the molten state by the physical arrest imposed on the polymer chains as a result of the intimate contact with the glass fibres, or alternatively by polar interactions of the carboxylic moieties in PLA with the hydroxyl groups on the fibre surface.

Pre-alignment of polymer chains near the fibre surface may account for the preferential occurrence of transcrystallinity in the cycled pressure composite series. At this stage, it is unclear if the relatively low crystallinity and the development of transcrystallinity in the PLA-PGF composite system leads to a beneficial effect on the interfacial shear strength in the CP composite series. Further studies on transcrystallinity in the PLA-PGF system and its effect on interfacial shear strength will be conducted to address this issue.

Despite the limitation of the processing temperatures to 180 °C and the thorough evacuation of moisture before processing, the chromatography results suggested that PLA was increasingly degraded throughout the manufacturing sequence as shown in Table 5.

Thermal degradation was more noticeable in the composites, especially in the 0.35 and 0.45 volume fractions, where the post-processing molecular weight decreased to ca. 85% and 80% of the number average molecular weight of virgin PLA respectively. The similarity between the neat PLA plate strength processed at 180 °C (75 ± 3 MPa) and the effective matrix strength in the composites (ca. 77 MPa), suggested that the mechanical properties of the matrix were not significantly altered due to molecular weight decrease associated with the matrix-fibre interactions at the processing temperature. This result is in good agreement with previous studies where no significant difference in strength and modulus were observed for PLA tensile specimens with molecular weight reductions in the order of 10^4 g mol^{-1} [59,60].

Due to the hygroscopic nature of the PLA and the high surface energy of phosphate glass fibres [61], both constituents tend to collect low energy compounds present in the local environment including water vapour and organic contaminants during placement in the compression moulding tool. Thus, the higher the volume fraction of the composite, the more moisture was likely to be present in the laminate before consolidation. Upon heating, the polymer melt reacts with the adsorbed water, leading to reduced molecular weight and mechanical properties [62,63].

Similar observations with respect to molecular weight decrease of PLA have been reported in the melt processing of particulate Bioglass® reinforced-PLA products [29,64]. In spite of the small filler content used in one of these studies (ca. 2 vol.%) a significant drop to ca. 30% of the original polylactic acid M_w was reported [64]. The reduction was also attributed to the severe hydrolytic reaction between PLA and the hydrated glass particles occurring at the processing temperatures. This effect, in addition to the poor glass/polymer interface and the porosity stemming from bubble generation during extrusion, led to composite mechanical properties lower than those of neat PLA [64].

The results presented here highlight the potential of the PGF-PLA system and the significant advantages of the implementation of cyclic pressure in compression moulding for the manufacture of structural composite products with optimum mechanical properties and limited thermal degradation.

Although this work was mainly concerned with polylactic acid-phosphate glass fibre composites, the effects of cyclic pressure here demonstrated are not restricted to this particular system and may find application in the manufacture of alternative thermoplastic products.

5. Conclusions

Totally bioresorbable fibre reinforced composite plates were manufactured via compression moulding following two different consolidation approaches, namely, cyclic and static pressure. It was determined that composites with void contents lower than 1% could be manufactured through both processes at least up to 0.35 volume fraction. Flexural strengths of composites manufactured through cyclic pressure were found to exceed the strength of the samples manufactured via static pressure profile by at least 30%. The difference became more pronounced as the fibre volume fraction increased, reaching a maximum value of ca. 50% for the composite samples with 0.45 fibre volume fraction. This effect on the strength of the composites was explained by the ability of pressure cycling to potentially affect the permeability of the fibre network through relaxation and reapplication of pressure, leading to improved impregnation with respect to the static pressure profile. It was suggested that implementation of pressure cycles could also have an effect on the melt viscosity and the capillary pressure.

Composite modulus proved to be independent of the pressure profile since the calculated values were identical within experimental error. The deviation of the modulus values from the ideal behaviour for the 0.35 and 0.45 volume fractions was attributed to the increasing

segregation of fibres within the composite, resultant of the increasing thickness of the fibre mats used.

Differences in the DSC traces suggested the preferential formation of transcrystallinity in all the composites of the CP series probably as a result of the local chain alignment induced by the pulsating motion. The persistence of distinctive changes in crystallisation behaviour could be attributed to the physical arrest imposed on the polymer chains as a result of the intimate contact with the glass fibres, or alternatively by polar interactions of the carboxylic moieties in PLA with the hydroxyl groups on the fibre surface.

PLA progressively degraded as a result of the exposure to temperatures higher than the melting point throughout the manufacturing process. It was observed that the presence of phosphate glass fibres accelerated the thermal degradation of PLA. The extent of the degradation was found to be dependent on the fibre content. The molecular weight of the polymer matrix progressively decreased as the fibre volume fraction increased reaching a minimum in the 0.45 volume fraction composite of ca. 80% of the virgin PLA as a result of high temperature hydrolytic reaction of PLA with moisture adsorbed on PGF surface.

Acknowledgements

The authors gratefully acknowledge the financial support of the EPSRC through the Centre for Innovative Manufacturing in Medical Devices (Grant No. EP/K029592/1) and the National Council of Science and Technology (CONACyT, Mexico).

References

[1] E.J. Lee, F.K. Kasper, A.G. Mikos, Biomaterials for tissue engineering, Ann. Biomed. Eng. 42 (2) (2013) 323–337.
[2] G. Daculsi, History of development and use of the bioceramics and biocomposites, in: V.I. Antoniac (Ed.), Handbook of Bioceramics and Biocomposites, Springer International Publishing: Cham. 2014, pp. 1–20.
[3] S. Affatato, A. Ruggiero, M. Merola, Advanced biomaterials in hip joint arthroplasty. A review on polymer and ceramics composites as alternative bearings, Compos. Part B 83 (2015) 276–283.
[4] A. Hoppe, V. Mourino, A.R. Boccaccini, Therapeutic inorganic ions in bioactive glasses to enhance bone formation and beyond, Biomater. Sci. 1 (3) (2013) 254–256.
[5] V. Mouriño, J.P. Cattalini, A.R. Boccaccini, Metallic ions as therapeutic agents in tissue engineering scaffolds: an overview of their biological applications and strategies for new developments, J. R. Soc. Interface 9 (68) (2012) 401–419.
[6] M. Zhou, S. Xu, Y. Li, C. He, T. Jin, K. Wang, H. Deng, Q. Zhang, F. Chen, Q. Fu, Transcrystalline formation and properties of polypropylene on the surface of ramie fiber as induced by shear or dopamine modification, Polymer 55 (13) (2014) 3045–3053.
[7] P. Nygard, C.-G. Gustafson, Continuous glass fiber–polypropylene composites made by melt impregnation: influence of processing method, J. Thermoplast. Compos. Mater. 17 (2) (2004) 167–184.
[8] A.E. Scott, I. Sinclair, S.M. Spearing, M.N. Mavrogordato, W. Hepples, Influence of voids on damage mechanisms in carbon/epoxy composites determined via high resolution computed tomography, Compos. Sci. Technol. 90 (2014) 147–153.
[9] T.S. Mesogitis, A.A. Skordos, A.C. Long, Uncertainty in the manufacturing of fibrous thermosetting composites: a review, Compos. A: Appl. Sci. Manuf. 57 (2014) 67–75.
[10] M. Stefanovska, B. Samakoski, S. Risteska, G. Maneski, Influence of some technological parameters on the content of voids in composite during on-line consolidation with filament winding technology international journal of chemical, biomolecular, metallurgical, Mater. Sci. Eng. 8 (5) (2014) 347–351.
[11] J.P. Anderson, M.C. Altan, Formation of voids in composite laminates: coupled effect of moisture content and processing pressure, Polym. Compos. 36 (2) (2015) 376–384.
[12] D. Garlotta, A literature review of poly(lactic acid), J. Polym. Environ. 9 (2) (2001) 63–84.
[13] A. Södergård, M. Stolt, Properties of lactic acid based polymers and their correlation with composition, Prog. Polym. Sci. 27 (6) (2002) 1123–1163.
[14] J.W. Seo, W.I. Lee, A model of the resin impregnation in thermoplastic composites, J. Compos. Mater. 25 (9) (1991) 1127–1142.
[15] L. Fambri, C. Migliaresi, Crystallization and Thermal Properties, in Poly(Lactic Acid), John Wiley & Sons, Inc., 2010 113–124.
[16] ASTM D2734-09, Standard Test Methods for Void Content of Reinforced Plastics, 2009.
[17] ASTM D792-13, Standard Test Methods for Density and Specific Gravity (Relative Density) of Plastics by Displacement, 2013.
[18] ASTM D2584-11, Standard Test Method for Ignition Loss of Cured Reinforced Resins, 2011.
[19] P.K. Mallick, Fiber-Reinforced Composites: Materials, Manufacturing, and Design, second ed. Taylor & Francis, 1993.
[20] U.K. Vaidya, K.K. Chawla, Processing of fibre reinforced thermoplastic composites, Int. Mater. Rev. 53 (4) (2008) 185–218.
[21] L. Liu, B.-M. Zhang, D.-F. Wang, Z.-J. Wu, Effects of cure cycles on void content and mechanical properties of composite laminates, Compos. Struct. 73 (3) (2006) 303–309.
[22] P.O. Hagstrand, F. Bonjour, J.A.E. Månson, The influence of void content on the structural flexural performance of unidirectional glass fibre reinforced polypropylene composites, Compos. A: Appl. Sci. Manuf. 36 (5) (2005) 705–714.
[23] J.L. Thomason, The interface region in glass fibre-reinforced epoxy resin composites: 1. Sample preparation, void content and interfacial strength, Composites 26 (7) (1995) 467–475.
[24] C. Mayer, X. Wang, M. Neitzel, Macro- and micro-impregnation phenomena in continuous manufacturing of fabric reinforced thermoplastic composites, Compos. A: Appl. Sci. Manuf. 29 (7) (1998) 783–793.
[25] E. Ruiz, V. Achim, S. Soukane, F. Trochu, J. Bréard, Optimization of injection flow rate to minimize micro/macro-voids formation in resin transfer molded composites, Compos. Sci. Technol. 66 (3–4) (2006) 475–486.
[26] P.K. Mallick, Composites Engineering Handbook, Taylor & Francis, 1997.
[27] Ahmadi, Z., S.R. G., Amiri, D., Continuous melt impregnation process: Materials parameters. Iran. Polym. J. (English) 2000. 9(2): pp. 125–130.
[28] J.J. Blaker, V. Maquet, A.R. Boccaccini, R. Jerome, A. Bismarck, Wetting of Bioactive Glass Surfaces by Poly(Alpha-Hydroxyacid) Melts: Interaction Between Bioglass (R) and Biodegradable Polymers, European Polymer Federation, 2005.
[29] T. Niemelä, H. Niiranen, M. Kellomäki, P. Törmälä, Self-reinforced composites of bioabsorbable polymer and bioactive glass with different bioactive glass contents. Part I: initial mechanical properties and bioactivity, Acta Biomater. 1 (2) (2005) 235–242.
[30] M.K. Kang, W.I. Lee, H.T. Hahn, Formation of microvoids during resin-transfer molding process, Compos. Sci. Technol. 60 (12 − 13) (2000) 2427–2434.
[31] N. Othman, B. Jazrawi, P. Mehrkhodavandi, S.G. Hatzikiriakos, Wall slip and melt fracture of poly(lactides), Rheol. Acta 51 (4) (2011) 357–369.
[32] J. Dorgan, H. Lehermeier, M. Mang, Thermal and rheological properties of commercial-grade poly(lactic acid)s, J. Polym. Environ. 8 (1) (2000) 1–9.
[33] Y. Xiao-chun, Z. Wen-bin, H. Guang-jian, Y. Zhi-tao, Q. Jin-ping, Influence of pressure oscillation on injection molding process, J. Thermoplast. Compos. Mater. 27 (10) (2014) 1417–1427.
[34] Z. Yan, K.Z. Shen, J. Zhang, L.M. Chen, C. Zhou, Effect of vibration on rheology of polymer melt, J. Appl. Polym. Sci. 85 (8) (2002) 1587–1592.
[35] G.S. Layser, J.P. Coulter, Localized effects of dynamic melt manipulation on flow induced orientation and mechanical performance of injection molded products, Polym. Eng. Sci. 47 (11) (2007) 1912–1919.
[36] J.P. Ibar, Control of polymer properties by melt vibration technology: a review, Polym. Eng. Sci. 38 (1) (1998) 1–20.
[37] H.A. Barnes, P. Townsend, K. Walters, On pulsatile flow of non-Newtonian fluid, Rheol. Acta 10 (1971) 517–527.
[38] I. Ahmed, I.A. Jones, A.J. Parsons, J. Bernard, J. Farmer, C.A. Scotchford, G.S. Walker, C.D. Rudd, Composites for bone repair: phosphate glass fibre reinforced PLA with varying fibre architecture, J. Mater. Sci. Mater. Med. 22 (8) (2011) 1825–1834.
[39] R.M. Felfel, I. Ahmed, A.J. Parsons, P. Haque, G.S. Walker, C.D. Rudd, Investigation of crystallinity, molecular weight change, and mechanical properties of PLA/PBG bioresorbable composites as bone fracture fixation plates, J. Biomater. Appl. 26 (7) (2012) 765–789.
[40] N. Han, I. Ahmed, A.J. Parsons, L. Harper, C.A. Scotchford, B.E. Scammell, C.D. Rudd, Influence of screw holes and gamma sterilization on properties of phosphate glass fiber-reinforced composite bone plates, J.Biomater. Appl. 27 (2011) 990–1002.
[41] N. Sharmin, M.S. Hasan, A.J. Parsons, C.D. Rudd, I. Ahmed, Cytocompatibility, mechanical and dissolution properties of high strength boron and iron oxide phosphate glass fibre reinforced bioresorbable composites, J. Mech. Behav. Biomed. Mater. 59 (2016) 41–56.
[42] M.S. Hasan, I. Ahmed, A.J. Parsons, G.S. Walker, C.A. Scotchford, The influence of coupling agents on mechanical property retention and long-term cytocompatibility of phosphate glass fibre reinforced PLA composites, J. Mech. Behav. Biomed. Mater. 28 (2013) 1–14.
[43] P. Olivier, J.P. Cottu, B. Ferret, Effects of cure cycle pressure and voids on some mechanical properties of carbon/epoxy laminates, Composites 26 (7) (1995) 509–515.
[44] R.C. Wetherhold, Statistical distribution of strength of fiber-reinforced composite materials, Polym. Compos. 7 (2) (1986) 116–123.
[45] R.M. Jones, Mechanics Of Composite Materials, Taylor & Francis, 1998.
[46] J.L. Thomason, A.A. van Rooyen, The transcrystallised interphase in thermoplastic composites, in: H. Ishida (Ed.), Controlled Interphases in Composite Materials, 423-430, Springer Netherlands, 1990.
[47] N. Le Moigne, M. Longerey, J.-M. Taulemesse, J.-C. Bénézet, A. Bergeret, Study of the interface in natural fibres reinforced poly(lactic acid) biocomposites modified by optimized organosilane treatments, Ind. Crop. Prod. 52 (2014) 481–494.
[48] H. Xu, L. Xie, X. Jiang, X.-J. Li, Y. Li, Z.-J. Zhang, G.-J. Zhong, Z.-M. Li, Toward stronger transcrystalline layers in poly(l-lactic acid)/natural fiber biocomposites with the aid of an accelerator of chain mobility, J. Phys. Chem. B 118 (3) (2014) 812–823.
[49] S. Han, K. Ren, C. Geng, K. Wang, Q. Zhang, F. Chen, Q. Fu, Enhanced interfacial adhesion via interfacial crystallization between sisal fiber and isotactic polypropylene: direct evidence from single-fiber fragmentation testing, Polym. Int. 63 (4) (2014) 646–651.
[50] A. Costantino, V. Pettarin, J. Viana, A. Pontes, A. Pouzada, P. Frontini, Microstructure of PP/clay nanocomposites produced by shear induced injection moulding, Procedia Materials Science 1 (2012) 34–43.

[51] M. Bilewicz, J.C. Viana, L.A. Dobrzański, Development of microstructure affected by in-mould manipulation in polymer composites and nanocomposites, Journal of Achievements in Materials and Manufacturing Engineering 31 (1) (2008) 71–76.
[52] G. Kalay, C. O., P.S. Allan, M.J. Bevis, The management of microstructure in semi-crystalline polymers, Chem. Eng. Res.Des. 73a (1995) 798–809.
[53] P. Pan, W. Kai, B. Zhu, T. Dong, Y. Inoue, Polymorphous crystallization and multiple melting behavior of poly(l-lactide): molecular weight dependence, Macromolecules 40 (19) (2007) 6898–6905.
[54] J.F. Mano, Y. Wang, J.C. Viana, Z. Denchev, M.J. Oliveira, Cold crystallization of PLLA studied by simultaneous SAXS and WAXS, Macromol. Mater. Eng. 289 (10) (2004) 910–915.
[55] N. Billon, J. Haudin, Influence of transcrystallinity on DSC analysis of polymers, J. Therm. Anal. Calorim. 42 (4) (1994) 679–696.
[56] G. Pompe, E. Mäder, Experimental detection of a transcrystalline interphase in glass-fibre/polypropylene composites, Compos. Sci. Technol. 60 (11) (2000) 2159–2167.
[57] Y. Chen, X. Wen, M. Nie, Q. Wang, Preparation of polypropylene/glass fiber composite with high performance through interfacial crystallization, J.Vinyl Addit. Technol. (2015) p. n/a-n/a.
[58] H. Quan, Z.-M. Li, M.-B. Yang, R. Huang, On transcrystallinity in semi-crystalline polymer composites, Compos. Sci. Technol. 65 (7–8) (2005) 999–1021.
[59] F. Carrasco, P. Pagès, J. Gámez-Pérez, O.O. Santana, M.L. Maspoch, Processing of poly (lactic acid): characterization of chemical structure, thermal stability and mechanical properties, Polym. Degrad. Stab. 95 (2) (2010) 116–125.
[60] Y. Ikada, H. Tsuji, Biodegradable polyesters for medical and ecological applications, Macromol. Rapid Commun. 21 (3) (2000) 117–132.
[61] A. Bismarck, A.R. Boccaccini, E. Egia-Ajuriagojeaskoa, D. Hülsenberg, T. Leutbecher, Surface characterization of glass fibers made from silicate waste: zeta-potential and contact angle measurements, J. Mater. Sci. 39 (2) (2004) 401–412.
[62] L.T. Lim, R. Auras, M. Rubino, Processing technologies for poly(lactic acid), Prog. Polym. Sci. 33 (8) (2008) 820–852.
[63] L.-T. Lim, K. Cink, T. Vanyo, Processing of Poly(Lactic Acid), in Poly(Lactic Acid), John Wiley & Sons, Inc., 2010 189–215.
[64] J.J. Blaker, A. Bismarck, A.R. Boccaccini, A.M. Young, S.N. Nazhat, Premature degradation of poly(alpha-hydroxyesters) during thermal processing of bioglass-containing composites, Acta Biomater. 6 (3) (2010) 756–762.